Determination of thermal material properties for the numerical simulation of cutting processes

Michael Storchak[1] · Thomas Stehle[1] · Hans-Christian Möhring[1]

Abstract
Thermal properties of machined materials, which depend significantly on the change in cutting temperature, have a considerable effect on thermal machining characteristics. Therefore, the thermal properties used for the numerical simulation of the cutting process should be determined depending on the cutting temperature. To determine the thermal properties of the machined materials, a methodology and a software-implemented algorithm were developed for their calculation. This methodology is based on analytical models for the determination of tangential stress in the primary cutting zone. Based on this stress and experimentally or analytically determined cutting temperatures, thermal properties of the machined material were calculated, namely the coefficient of the heat capacity as well as the coefficient of thermal conductivity. Three variants were provided for determining the tangential stress: based on the yield stress calculated using the Johnson-Cook constitutive equation, based on the experimentally determined cutting and thrust forces as well as by directly calculating the tangential stress. The thermal properties were determined using the example of three different materials: AISI 1045 and AISI 4140 steel as well as Ti10V2Fe3Al titanium alloy (Ti-1023). With the developed FE cutting model, the deviation between experimental and simulated temperature values ranged from approx. 7.5 to 14.4%.

Keywords Cutting · Thermal properties · Simulation

1 Introduction

As one of the main methods of shaping various products, providing their necessary accuracy and manufacturing quality, the cutting process has been the subject of study by numerous researchers for many decades. One of the most powerful tools for studying cutting has been the process of its modeling. Particular advances have been made in the development of numerical cutting models, e.g., using the finite element method [1] and also mesh-free methods [2]. In recent decades, this method is often successfully used to study the characteristics of the cutting process [3, 4] in particular the kinetic [5] and thermal [6] characteristics, tool wear [7], physico-mechanical characteristics of the workpiece boundary layers [8, 9], etc.

In order to be able to apply numerical cutting models, numerous studies have been carried out to create the components of the FE-model triad: a model of the machined material (the constitutive equation), a friction model, and a fracture model of the machined material. Significant efforts have been made to determine material models suitable for numerical cutting models [10], as well as methods for calculating the constitutive equation parameters [11, 12]. Significant advances have been made in evaluating the contact interaction between the tool and chip and the workpiece [13, 14] and in developing friction models that characterize this interaction [11, 15]. A detailed study of the machined material fracture and chip forming processes [5] has contributed to the development of various models of machined material fracture (see e.g., [16, 17]). This ensured the development of fracture models for various hard-to-machine steels and titanium alloys during cutting [18–20].

Despite significant successes in applying numerical models to predict the cutting process characteristics, the simulation results differ from the corresponding experimental data. In order to obtain machining characteristics corresponding to the specific modeled processes of material removal, it is necessary to use realistic values of cutting model parameters. Whereas there has been extensive research into establishing

✉ Michael Storchak
   michael.storchak@ifw.uni-stuttgart.de

[1] Institute for Machine Tools, University of Stuttgart, Stuttgart, Germany

the parameters of the material model, the friction model, and the fracture model of the machined material, little attention has been given to determining the thermal properties of the material for modeling the cutting process. Yet, the thermal properties of the material to be machined have a significant impact on the cutting process characteristics and, particularly on the value of the cutting temperature. The simulation of cutting temperature, along with other important characteristics of the cutting process, is given special attention. The thermal properties of the materials to be machined have a predominant influence on the temperature distribution in the various cutting zones [21, 22]. A significant influence of thermal properties has been established on the constitutive equation parameters used to the machined material model [23], on, for example, predicting the cutting temperature for complex tool cutting wedge shapes [24], when machining difficult-to-machine steels and titanium alloys [25], when using tools with coatings [26], etc.

This paper presents studies into establishing the thermal properties of the machined materials, especially for the modeling of cutting processes. In addition, a method for determining these properties and the simulation results of cutting temperature are described here using the example of orthogonal cutting.

2 Methods for the determination of thermal properties

Fundamental material properties, such as mechanical and thermal properties, are a necessary part of every cutting model of these materials. Determining the thermal properties of materials has been a research subject for a long time. During this period, well-established methods and procedures for determining thermal properties have been developed. The basic procedures for determining these properties specifically for material removal processes are outlined in a review by Davies and colleagues [27]. Most publications on the modeling of cutting processes have taken the thermal properties of the machined material from the constant values included as standard in the simulation software (see e.g., [28–32]). In the studies dealing with the analytical modeling of cutting processes (see e.g., [22, 29, 33–36]), the properties required have been established as constant values based on similar sources.

The thermal properties of materials have mainly been determined by experiment (see e.g., [37–39]). However, there have also been experiments to establish these properties theoretically or analytically [40, 41] as well as to numerically simulate and calculate the thermal properties of different kinds of steel (see e.g., [42]). These values have been determined with common methods for the examination of material properties (see [38, 43–46] and many others).

The values of the thermal properties have been established at a fixed temperature of the material, mainly at room temperature. In addition, it is known that the thermal properties of materials such as specific heat, thermal expansion, and thermal conductivity also change significantly with varying temperature of the examined material [37, 38, 40]. If it is not taken into consideration that the thermal properties of the machined material change when its temperature changes, fundamental errors occur regarding the determination of thermal flows in this material. In turn, this leads to considerable errors when establishing the temperature and the kinetic characteristics of cutting processes, tool wear, etc.

In rather less known studies, changes in the thermal properties of the machined material with varying temperature have been taken into account [1]. A procedure has been developed to summarize the data on the change in the thermal properties of the machined material depending on its temperature in a table. In this case, the values of thermal properties from the table corresponding to a certain cutting temperature are used to simulate the cutting process (see e.g., [1, 47]). The temperature dependences of the thermal properties of materials obtained experimentally or by calculation are also approximated by equations of the first [36] or higher orders [48, 49].

Based on the above analysis, it can be concluded that the known methods for determining the thermal properties of machined materials are based on the assumption that the thermal properties to be determined are constant within the boundaries of the test specimen. However, during cutting, the machined material is under conditions in which its thermal properties change and depend on the stress-strain state of that material (see below). This must be taken into account when determining the thermal properties of materials in order to use these properties in the cutting process simulation.

3 Methodology for identifying thermal properties

The specific characteristic of the material deformation and the subsequent material breaking during the cutting in heterogeneous shearing processes is that areas with different states of stress-strain arise and thus with a considerably different deformation in corresponding cutting zones [50–52]. In the same way, the temperature of the material in the cutting zones and their areas differs considerably [30, 53, 54]. Under certain cutting conditions, this leads to a hardening of the material as well as to a softening of the material among other things. The thermal properties of the material and how they vary with temperature depend basically on its state of stress-strain. The condition of the material in different cutting zones differs greatly from the usual, often undeformed

condition in which its thermal properties are generally measured. As such material conditions can only be obtained during the cutting process [52], the thermal properties of the material have to be established during the corresponding machining processes.

For establishing the thermal properties of the machined material, which are necessary to simulate different cutting processes, it was suggested to determine by experiment the cutting temperature in the respective zones based on the analytical description of the stress-strain state of the material [51, 52] in the cutting zones — Fig. 1. In this case, it was necessary to find out for which area or rather cutting zone the corresponding calculations and temperature measurements must be carried out. Naturally, it made sense to choose that cutting zone or that area of the zone in which there is a constant temperature distribution, the measuring point is as accessible as possible and the measuring process itself is comfortable on the whole. A constant temperature distribution depends basically on a homogeneous stress-strain state of the material [52, 53, 55]. A homogeneous stress-strain state of the machined material and a resulting constant temperature occurs in those cutting zones with predominantly adiabatic deformation conditions leading to material hardening or isothermal deformation conditions leading to material softening. Under these conditions, the material is only in the primary cutting zone [52, 56]. In this zone, the material to be machined is under all-around compression. This condition provides for a uniform distribution of deformations, stresses, and temperatures throughout the entire primary cutting zone. Possible irregularities in the distribution of these characteristics accompanying the machining of such difficult-to-machine materials as, for example, titanium and nickel alloys, austenitic steels, etc., arise after the material to be machined has left the primary cutting zone, i.e., after the final chip formation. This occurs already in the stagnant area of the secondary cutting zone [52, 56].

The temperature distribution within the primary zone, inside the area bounded by the indicated temperature isolines (see Fig. 1), is approximately constant compared with the temperature distribution in the secondary and tertiary cutting zones, in which there is a temperature gradient of up to 5 °C/μm [27, 53, 54, 57]. Moreover, the accessibility to the temperature measurement of the primary cutting zone is considerably better and more comfortable than in other cutting zones, because the temperature can be measured at the exterior surface of the chip during the transition from workpiece material to chip (see Fig. 1). For example, the temperature at the exterior surface of the chip in this measuring point is the same as in the primary cutting zone. This occurs if the chip thickness is within the conventional range, the chip forming process is constant, and the temperature at this measuring point has reached the steady-state condition [55, 58].

The temperature of the deformed material in the primary cutting zone was in proportion to the specific deformation work [52, 53]:

$$T_{d0} = \frac{A_w}{C_V} \cdot K_{P\varepsilon} = \frac{\tau_t \cdot \varepsilon_w}{C_V} \cdot K_{P\varepsilon}, \tag{1}$$

where A_w is the specific deformation work, C_V is the coefficient of the specific volumetric heat capacity of the machined material, τ_t is the tangential stress in the primary cutting zone or rather the specific tangential force in this zone, ε_w is the true final strain, and $K_{P\varepsilon}$ is the coefficient of heat flow from the primary cutting zone into the workpiece.

The true final strain ε_w in the case of adiabatic material hardening was established with the chip compression ratio K_a [12, 50, 51]:

$$\varepsilon_w = \frac{K_a + \frac{1}{K_a} - 2 \cdot \sin\gamma}{\cos\gamma}, \quad K_a = \frac{a_C}{a} \tag{2}$$

where a is the undeformed chip thickness (depth of cut), a_c is the chip thickness, and γ is the tool orthogonal rake angle of the tool wedge (see Fig. 1).

The coefficient of heat flow from the primary cutting zone into the workpiece $K_{P\varepsilon}$ was defined by the following equation [52]:

$$K_{P\varepsilon} = \frac{1}{1 + \frac{1 - e^{-P_e \cdot \tan\phi}}{P_e \cdot \tan\phi}} = \frac{1}{1 + \frac{\cot\phi}{P_e}}, \tag{3}$$

$$P_e = \frac{V_C \cdot a}{\omega}, \tag{4}$$

where, P_e is the Péclet number (Péclet criterion), ϕ is the shear angle, V_C is the cutting speed, and ω is the coefficient of
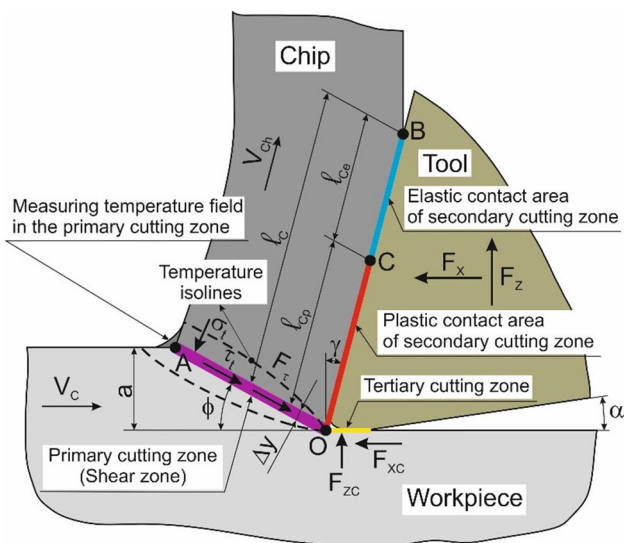

Fig. 1 Layout of cutting zones

thermal diffusivity, defined as the quotient of the coefficient of thermal conductivity and the coefficient of specific volumetric heat capacity.

The shear angle ϕ was determined using the chip compression ratio K_a and the tool orthogonal rake angle γ:

$$\phi = \arctan\left(\frac{\frac{1}{K_a} \cdot \cos\gamma}{1 - \frac{1}{K_a} \cdot \sin\gamma}\right). \tag{5}$$

As the temperature at the exterior surface of the chip (see Fig. 1) was established by experiment, the coefficient of the specific volumetric heat capacity C_V could be calculated as follows:

$$C_V = \frac{\tau_t \cdot \varepsilon_w \cdot K_{P\varepsilon}}{T_{\text{dmeas}}} \tag{6}$$

The stress-strain state of the machined material in the primary cutting zone during cutting could be clearly established with the tangential stress or rather the specific tangential force τ_t (see Fig. 1) and the true final strain ε_w [50–52]. The tangential stress τ_t was determined in three different ways:

➢ Due to the yield stress σ_t calculated using a well-known constitutive equation (e.g., Johnson-cook [59]) (JC);
➢ Based on the resultant forces determined by experiment, e.g., F_x and f_z in the case of orthogonal cutting (MF);
➢ By directly calculating the tangential stress τ_t (TS).

According to the first method (JC), the yield stress σ_t prevailing in the primary cutting zone during the machining of material was established using a constitutive equation, in this case with the Johnson-Cook constitutive equation [59]:

$$\sigma_t = (A + B \cdot \varepsilon^n) \cdot \left[1 + C \cdot \ln\left(\frac{\dot{\varepsilon}}{\dot{\varepsilon}_0}\right)\right] \cdot \left[1 - \left(\frac{T_{\text{dmeas}} - T_r}{T_m - T_r}\right)^m\right] \tag{7}$$

where σ_t is the yield stress, A is the initial yield stress, B is the stress coefficient of strain hardening, n is the power coefficient of strain hardening, C is the strain rate coefficient, m is the power coefficient of thermal softening, ε is the strain, $\dot{\varepsilon}$ is the strain rate, $\dot{\varepsilon}_0$ is the reference value of strain rate, T_{dmeas} is the actually measured temperature in the primary cutting zone, T_r is the reference or room temperature, and T_m is the melting temperature of the material to be machined (machined material).

The constitutive equation contains five constants: A, B, n, C, and m, which can be determined by experiment (see e.g., [12]). The tangential stress τ_t was calculated through the yield stress σ_t as follows [12, 52]:

$$\tau_t = \frac{\sigma_t}{\sqrt{3}} \tag{8}$$

The strain rate $\dot{\varepsilon}$ from Eq. (7) could be calculated in two different ways, either due to Oxley's machining theory [12, 50, 60–62]:

$$\dot{\varepsilon} = \frac{C_0 \cdot V_C \cdot \cos\gamma \cdot \sin\phi}{\sqrt{3} \cdot a \cdot \cos(\phi - \gamma)}, \tag{9}$$

where C_0 is the thickness ratio of the primary cutting zone, or due to Zorev's machining theory [12, 51]:

$$\dot{\varepsilon} = \frac{V_C \cdot \cos\gamma}{\sqrt{3} \cdot \Delta y \cdot \cos(\phi - \gamma)}, \tag{10}$$

where Δy is the thickness of the primary cutting zone (see Fig. 1).

If it was considerably difficult or impossible to directly measure the thickness of the primary cutting zone Δy, the value was determined with the following inequality [12]:

$$\frac{a}{10 \cdot \sin\phi} \leq \Delta y \leq \frac{a}{2 \cdot \sin\phi}. \tag{11}$$

Instead of using the classic Johnson-Cook equation, it would also be possible to apply the modified equations developed in the last years (see e.g., [63–65]).

According to the second method (MF), the tangential stress τ_t in the primary cutting zone was determined due to the resultant forces established by experiment [51, 52]:

$$\tau_t = \frac{(F_X - F_{XC}) \cdot \cos\phi - (F_Z - F_{ZC}) \cdot \sin\phi}{a \cdot w} \cdot \sin\phi, \tag{12}$$

where w is the cutting width, F_X and F_Z are the experimental cutting and thrust forces respectively (in the case of orthogonal cutting), and F_{XC} and F_{ZC} are the cutting and thrust forces at the clearance face of the tool wedge (in the tertiary cutting zone) respectively.

The forces F_{XC} and F_{ZC} in the tertiary cutting zone are determined by extrapolating the dependence of respective forces on the depth of cut to the zero value of this depth of cut [51, 56, 66].

In the third method (TS), the tangential stress τ_t was directly calculated according to the following equation [52]:

$$\tau_t = \begin{cases} R_t \cdot e^{-m_h \cdot \left(\frac{\varepsilon_w}{\varepsilon_{\tau\max}} - 1\right)} \cdot \left[\varepsilon_{\tau\max}^{m_h} \cdot \frac{K_\varepsilon \cdot A}{1+m_h} \cdot \left(1 - \frac{\varepsilon_{\tau\max}}{\varepsilon_w}\right) + \frac{\ln(1+m_h)}{A_1 \cdot B_\tau \cdot \varepsilon_w}\right], & \varepsilon_w > \varepsilon_{\tau\max} \\ R_t \cdot \ln\left(1 + \frac{A \cdot A_1 \cdot B_\tau \cdot K_\varepsilon}{1+m_h} \cdot \varepsilon_w^{m_h+1}\right) \cdot \frac{1}{A_1 \cdot B_\tau \cdot \varepsilon_w}, & \varepsilon_{\tau\max} > \varepsilon_w \end{cases} \tag{13}$$

where R_t is the true ultimate strength, m_h is the empirically established parameter of the material deformation hardening, B_τ is the empirical constant taking account of the joint effect of strain rate and temperature on the yield

point, and K_ε is the empirical constant regarding the effect of the strain rate at a partly constant mean temperature. The dimensionless complexes A_1 and A were defined with the following equation [52, 53, 56]:

$$A = \frac{1}{\sqrt{3} \cdot \left[\sqrt{3} \cdot \ln\left(1 + \delta\right) \right]^{m_h}}, \tag{14}$$

$$A_1 = \frac{R_t}{C_V \cdot T_m} \tag{15}$$

The experimental coefficients B_τ and K_ε were established using mechanical tensile/compression tests according to the methodology in [12, 52]. The maximum deformation of the machined material to be reached under isothermal deformation conditions in the primary cutting zone was calculated with the following equation [53, 56]:

$$\varepsilon_{\tau \max} = \left[\frac{m_h \cdot \left(1 + m_h\right)}{A \cdot A_1 \cdot K_\varepsilon \cdot B_\tau} \right]^{\frac{1}{1+m_h}}, \tag{16}$$

However, the coefficient of mass specific heat capacity C_m is mostly used in commercial and other software for the simulation of machining processes. C_m of C_V was converted according to the following equation:

$$C_m = \frac{C_V}{\rho}, \tag{17}$$

where ρ is the density of the material.

By defining the coefficient of the specific heat capacity, it was possible to determine a further thermal property of the machined material, namely the coefficient of thermal conductivity λ. Zorev*s machining theory [51] and the extended Oxley's machining theory [12, 50, 60–62] were used for that. Based on the mathematical composition of the theory, the coefficient of thermal conductivity λ was calculated with the following system:

$$\begin{cases} \lambda = \frac{\rho \cdot C_m \cdot V_C \cdot a \cdot \tan\phi}{10^{\frac{0.5-\beta}{0.35}}}, 0.4 \le R_T \cdot \tan\phi \le 10.0 \\ \lambda = \frac{\rho \cdot C_m \cdot V_C \cdot a \cdot \tan\phi}{10^{\frac{0.3-\beta}{0.15}}}, R_T \cdot \tan\phi > 10.0 \end{cases} \tag{18}$$

The proportion of heat conducted into the workpiece β (a similar quantity like the coefficient of heat flow from the primary cutting zone into the workpiece $K_{P\varepsilon}$, see Eq. (3)) was calculated with the following equation:

$$\beta = 1 - \frac{\left(T_{\mathrm{dmeas}} - T_r\right) \cdot \cos\left(\phi - \gamma\right) \cdot \rho \cdot C_m \cdot a \cdot w}{F_\tau \cdot \cos\gamma \cdot \eta}, \tag{19}$$

in addition, the thermal number R_T was determined as follows:

$$R_T = \frac{\rho \cdot C_m \cdot V \cdot a}{\lambda}, \tag{20}$$

where η is the parameter to scale the average temperature rise at the shear plane (when fulfilling the conditions of orthogonal cutting).

The cutting force $F\tau$ (see Fig. 1) acting in the primary cutting zone was defined as follows:

$$F_\tau = \frac{\tau_t \cdot a \cdot w}{\sin\phi} \tag{21}$$

The sequence of steps in the procedure for determining the thermal properties of the materials subjected to the cutting process is shown in Fig. 2.

The coefficient of thermal expansion, which is also necessary for simulating cutting processes, can be established using a simulation-aided design of experiments (DOE) (not presented in this paper). The DOE method is determined based on the temperatures measured in the primary cutting zone as well as the coefficients of specific heat capacity C_V and thermal conductivity λ defined in advance (see Chapter 6).

4 Test setup

The device for conducting the experimental analyses was designed and assembled for establishing the cutting temperature at the exterior surface of the chip in the terminal
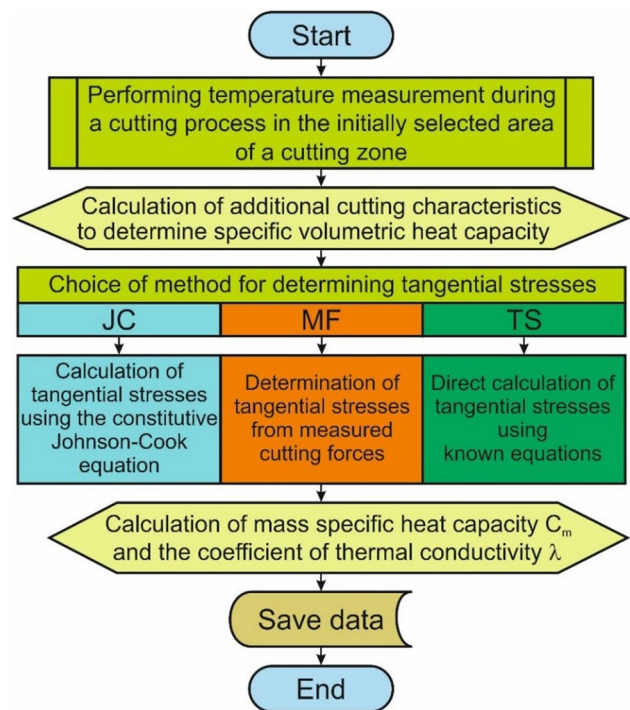

Fig. 2 Flowchart of the procedure for determining the thermal properties of the machined materials

area of the primary cutting zone. The measuring device consisted of two setups: one for conducting the cutting tests and one for the calibration of the measuring system.

4.1 Cutting tests

The experimental investigations into the determination of cutting temperatures were carried out in the machining of AISI 1045 and AISI 4140 steel as well as Ti-1023 titanium alloy (Ti10V2Fe3Al) using the test stand for orthogonal and oblique cutting [55, 66]. Fig. 3 shows the used test facility
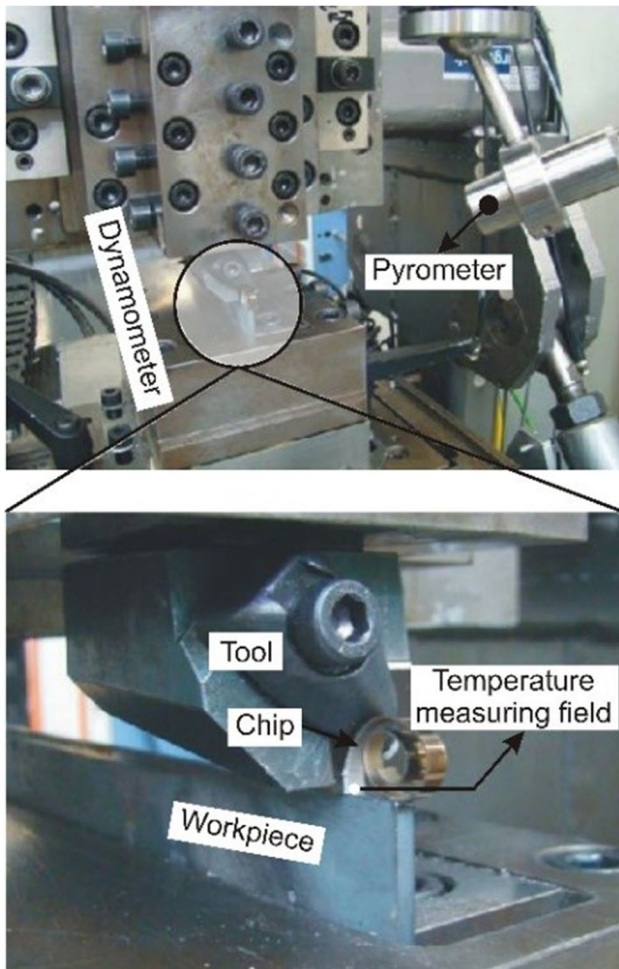

Fig. 3 Experimental setup for temperature measurement [58]

with the measuring equipment for establishing the resultant forces and cutting temperatures [58, 66]. The workpiece was clamped into a three-component dynamometer, type 9263 by Kistler, which was used for measuring the resultant forces. The cutting process was carried out using the tool with a clamped changeable cemented carbide insert SNMG-SM-1105 by Sandvik Coromant. The geometry of the tool wedge necessary for cutting was guaranteed by positioning and grinding the tool orthogonal clearance of the wedge. The tool orthogonal clearance was 8°, and the radius of cutting edge rounding was 20 μm in all tests. The tool orthogonal rake angle was changed from − 10° to 10° in steps of 10° in order to guarantee different values of the true final strain ε_w of the machined material in the primary cutting zone.

The cutting temperature was measured with a high-speed pyrometer, IGA-740 LO by LumoSense, at the exterior surface of the chip (see the measuring field in Fig. 3). The measuring field of the pyrometer ranged from 0.5 to 0.8 mm. The time resolution was 6 μsec. The cutting parameters used in the experiments are given in Table 1.

To carry out experimental studies, the area of cutting parameters for each studied material was selected separately. These cutting parameters are typically used in practice for turning, drilling, and milling AISI 1045 and AISI 4140 steels as well as the Ti-1023 titanium alloy. Specific values of cutting speeds from the commonly used in practice range are selected in such a way as to provide an integer value of the Péclet criterion. This criterion is further used as a similarity criterion for comparing cutting temperatures.

4.2 Calibration

During the cutting process, the machined material is subject to a considerable thermomechanical effect, which substantially changes not only the physical-mechanical properties of boundary layers, but also the topography of the workpiece surface and the chip. This greatly changes the emissivity of the surface to be measured. To take account of this phenomenon in the determination of the cutting temperature, the measuring system must be calibrated together with the measuring instruments for optically establishing the cutting temperature. This also concerned the temperature determination at the exterior surface of the chip in the accessible area of the primary cutting zone (s. Fig. 1 and Fig. 3).

Table 1 Cutting parameters in experimental tests

Material	Cutting speed, V_C [m/min]			Depth of cut, a [mm]			Péclet number, P_e [-]	
	Max.	Min.	Step	Max.	Min.	Step	Max.	Min.
AISI 1045	192	48	48	0.2	0.1	0.05	80	10
AISI 4140	144	48	48	0.2	0.1	0.05	60	10
Ti-1023	96	32	16	0.15	0.05	0.05	30	3.34

The fundamentals for establishing the temperature in cutting processes with different methods have been described in detail, e.g., in studies by G. Barrow [67] and G. W. Burns with M. G. Scroger [68]. In principle, there are two fundamentally different measuring methods for determining the temperature: contact and contactless methods [69]. The contact methods can be divided into stationary and dynamic methods. In the case of stationary methods, different thermosensors are used for the measurements [55]. With the dynamic methods, the temperature is measured using the tool and the workpiece, which are electrically isolated from each other but in contact during the measurement. Various techniques are used to calibrate the thermosensors as well as the tool-workpiece pair (see e.g., [70–74]). The contact methods are rarely applied for temperature measurements due to the great inertia of the used sensors and the considerable difficulties in placing such measuring elements as close to the cutting zones as possible [75].

In the last years, fiber-optic two-color pyrometers have been used for establishing the cutting temperature [76]. The principle is based on double measurements of the surface emissivity at two different wavelengths in the infrared range. When assuming that the object to be measured is a grey body of which the emissivity is independent from the wavelength, it is possible to evaluate the temperature and the emissivity of the chip surface using this method. Several measurements of cutting temperatures were carried out with such a two-color pyrometer [47, 77]. When the temperature was determined at the exterior surface of the chip, the surface to be measured was, however, not similar to the grey body and thus dependent on the wavelength [75]. In addition, it was very difficult or nearly impossible to orientate the measuring part of the glass fiber of the two-color pyrometer towards the measuring field. Measuring methods with pyrometers or thermographic cameras are better suited to measure the temperature at the exterior surface of the chip [75, 78–80]. The measuring system must be calibrated here with real test objects used in the experiments (exterior surface of a chip) as well as their surface properties. This method [75] [81] was used to calibrate the measuring system for the temperature determination.

The fundamental scheme for calibrating the measuring system is shown in Fig. 4. The pyrometer measured the temperature at the surface of the real chip during this calibration. This real chip was put on a heating unit and heated up to a set temperature using two heating elements. In addition to the pyrometer, the actual temperature in the heating unit and the chip was measured simultaneously using a calibrated thermosensor, type PT-100. Due to the signal of the actual temperature, a control signal was produced using the control program worked out in the environment of the LabVIEW software. Based on this signal, the power regulator, type M 028N, in the control unit created the desired
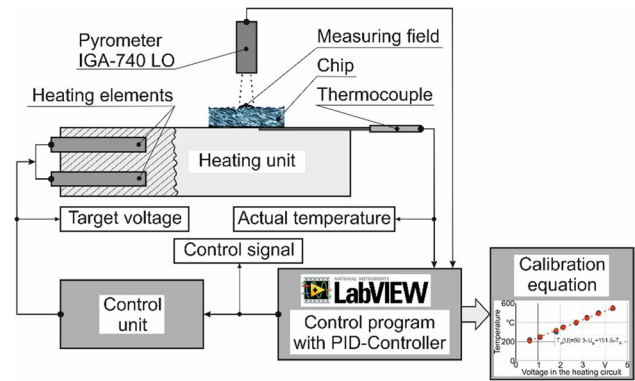

Fig. 4 Scheme for calibrating the measuring system

voltage with which the heating elements were fed. Thus, the heating elements warmed up the heating unit with the chip to a temperature set in the control program. The PID controller (proportional-integral-derivative controller) integrated into the LabVIEW control program ensured that the set temperature of the heating unit with the chip could be kept reliably.

By comparing the signal of the pyrometer with the temperature of the chip, it was possible to create a calibration equation using the LabVIEW program. Fig. 5 presents an example for the calibration equation regarding the temperature measurement at the exterior surface of the chip in the machining of AISI 1045 steel.

This method of calibration using real chips obtained during experimental studies provided the possibility for eliminating uncertainty when measuring the temperature in the transition area from the primary cutting zone to the exterior surface of the chip.

5 Experimental tests

The experimental tests for establishing the temperature at the exterior surface of the chip (see Fig. 1) were carried out applying the cutting parameters listed in Table 1. As an example, Fig. 6 shows the temperatures at the exterior surface of the chip measured during the orthogonal cutting of three test materials: AISI 1045 (Fig. 6, a), AISI 4140 (Fig. 6, b), and Ti-1023 (Fig. 6, c).

The temperature development is described depending on the different values for the true final strain of the machined material in the primary cutting zone and on the different Péclet numbers. It has to be noted here that the presented temperatures were interpolated to rounded values of true final strain. This was necessary in order to be able to compare the temperatures for different Péclet numbers.

The temperature at the exterior surface of the chip increased monotonously with rising true final strain. In the case of cutting processes with higher Péclet numbers,

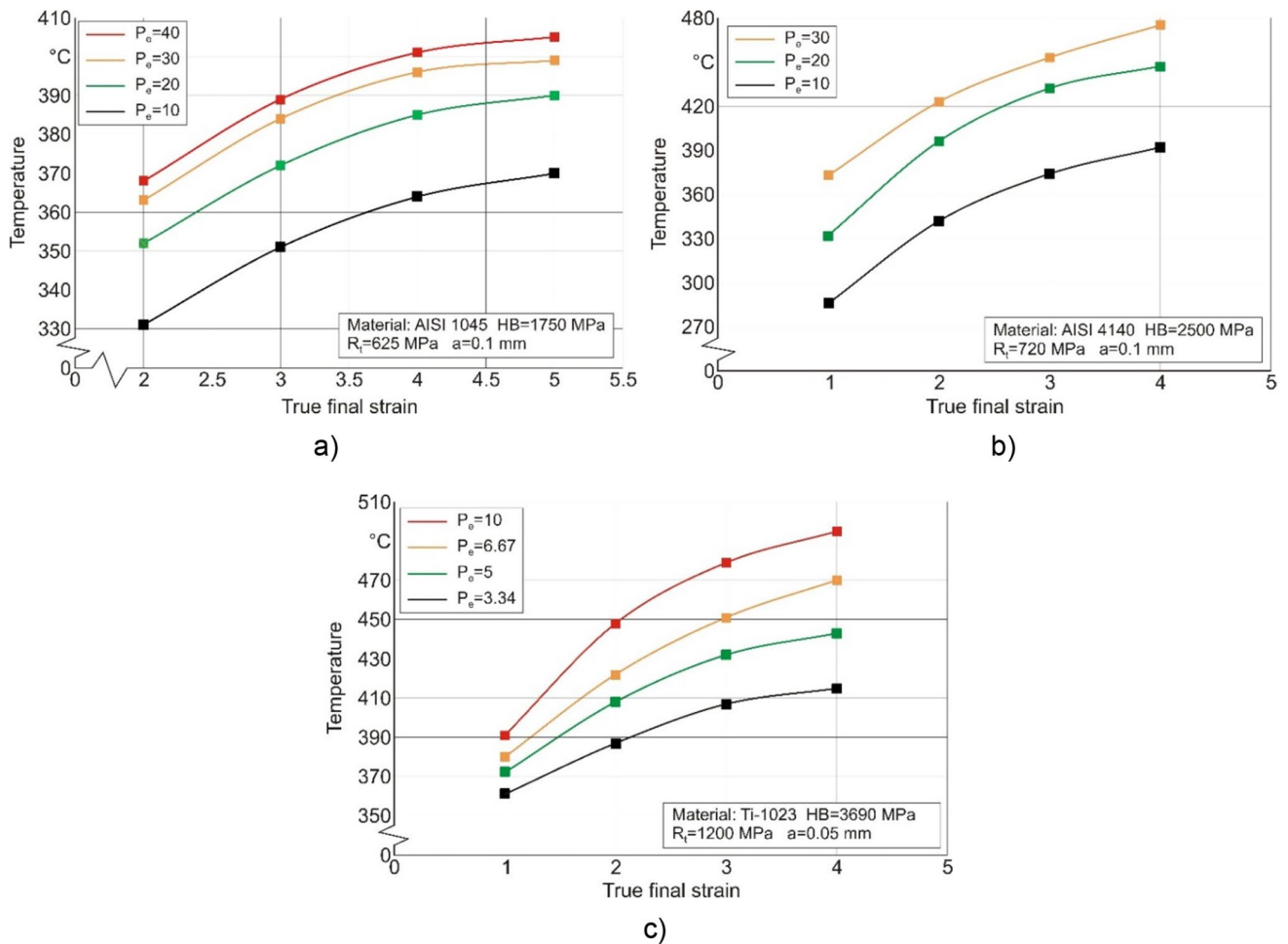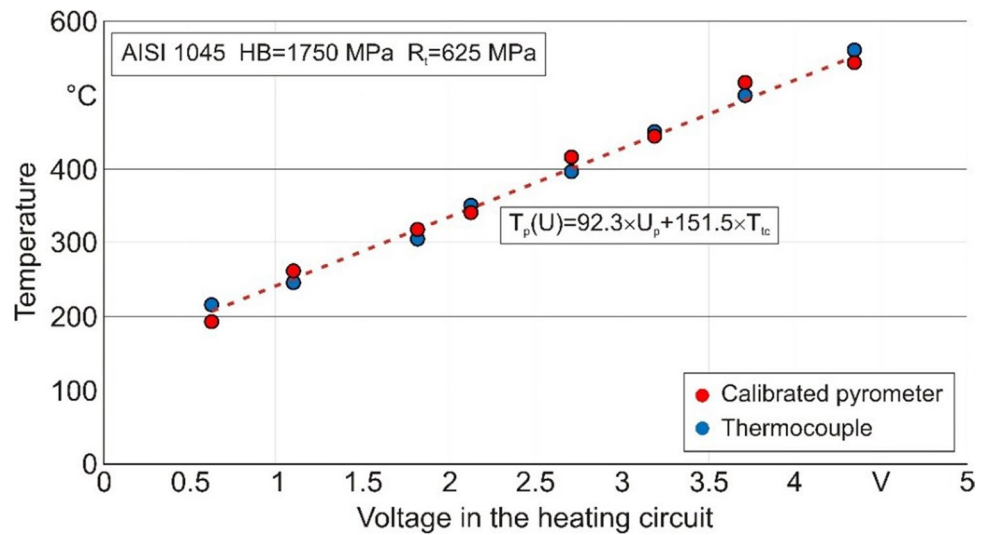**Fig. 5** Determination of the calibration equation

$$T_p(U) = 92.3 \times U_p + 151.5 \times T_{tc}$$

Material: AISI 1045 HB=1750 MPa R_t=625 MPa a=0.1 mm

a)

Material: AISI 4140 HB=2500 MPa R_t=720 MPa a=0.1 mm

b)

Material: Ti-1023 HB=3690 MPa R_t=1200 MPa a=0.05 mm

c)

Fig. 6 (**a**, **b**, **c**) Temperature at the exterior surface of the chip

the temperature reached considerably greater values. The change in true final strain necessary for the experimental tests was obtained by correspondingly different values of tool orthogonal rake angle γ and chip compression ratio K_a (see Eq. (2)). The different Péclet numbers were guaranteed by a change in cutting speed V_C and undeformed chip thickness or depth of cut a (see Eq. (4)).

As expected, the temperature in the cutting of heat-treatable steel AISI 1045 was considerably lower than in the machining of AISI 4140 high-alloy steel for corresponding values of true final strain and the Péclet number. This difference was also caused among other things by the substantial difference in the hardness of the steel materials. Regarding the materials examined in this study, the highest temperature occurred in the cutting process of Ti-1023 titanium alloy. This could be attributed to the considerably greater values of the true ultimate strength R_t and the hardness of the material. It was also not insignificant for the process of temperature development that the toughness was considerably greater than in the case of steel materials.

All tests carried out in this study with regard to the temperature at the exterior surface of the chip in the area of the primary cutting zone showed the same character as the results depicted as examples in Fig. 6. These were used further for establishing the desired thermal properties of the machined material.

6 Determination of thermal material properties

The methodology described in Chapter 3 was used for calculating the coefficient of volumetric heat capacity C_V or mass-specific heat capacity C_m as well as the coefficient of thermal conductivity λ of the machined material. The coefficients were determined for all three calculation variants: due to the Johnson-Cook constitutive equation (JC), based on resultant forces established by experiment (MF) and using directly calculating the tangential stress (TS) in the primary cutting zone (s. Chapter 3).

The parameters of the Johnson-Cook constitutive equation [59] were established for the examined materials using the method in [12] and listed in Table 2. According to this method, the parameters of the constitutive equation are determined separately. The values of the initial yield stress A, the stress coefficient of strain hardening B, and the power coefficient of strain hardening n are determined by fitting the flow curve in compression of samples at room temperature. Then, the samples are compressed at various temperatures up to the maximum cutting temperature. The average value of the power coefficient of thermal softening m is determined by appropriate processing of the obtained flow curves for the studied material. Finally, the strain rate coefficient C

Table 2 Johnson-Cook constitutive equation parameters [12, 82]

Material	A [MPa]	B [MPa]	n [-]	C [-]	m [-]
AISI 1045	439.125	475.9	0.2136	0.0181201	0.848
AISI 4140	632.3	546	0.1784	0.0175	1.46
Ti-1023	976.9	502.3	0.2214	0.02812	0.8

is determined for the conditions of the cutting process. To determine this coefficient, experimental studies of cutting forces are carried out, mainly during the orthogonal cutting process. The tangential stresses in the primary cutting zone are calculated from the obtained cutting forces. Based on the tangential stresses and taking into account the previously defined parameters of the constitutive equation, the coefficient C is calculated [12]. Thus, the coefficient C is determined for the strain rate range corresponding to the cutting conditions.

These values of the parameters were used for calculating the thermal properties of the machined material according to the first variant.

Table 3 shows the dependences of the coefficient of mass-specific heat capacity C_m and the coefficient of thermal conductivity λ on different values of final strain ε_w and calculation variants for the analyzed materials, using one value of the Péclet number and the depth of cut as an example.

When comparing the presented dependences, it could be noted that both coefficients C_m and λ increase with growing true final strain ε_w. The final strain of the machined material in the primary cutting zone during machining and the calculation variant affected the calculated values of both coefficients in fundamentally different ways. This effect also differed from material to material (s. Table 3). How much and in which way these influences had an effect differed with the change in cutting parameters, the chemical composition as well as the mechanical properties of the machined material, the tool geometry, and other cutting conditions. When analyzing the correlations between the thermal properties of the machined material, which have to be established, and the above-mentioned process parameters, it appeared that they have a unique character in every single case. Hence, it would be hardly possible to generalize them. That would require calculating the thermal properties of the machined material in every case to be conducted for the simulation. Regarding the completely structured analytical model for establishing these properties (see Chapter 3), the calculation method is suited well for the programming. Thus, the thermal properties required for simulating the cutting process could be calculated easily and reliably.

The use of the proposed three methods for determining the tangential stress ensures that the thermal properties of the machined materials are sufficiently close (see Table 3). This demonstrates that each of the three

Table 3 Calculated values of the thermal properties C_m and λ
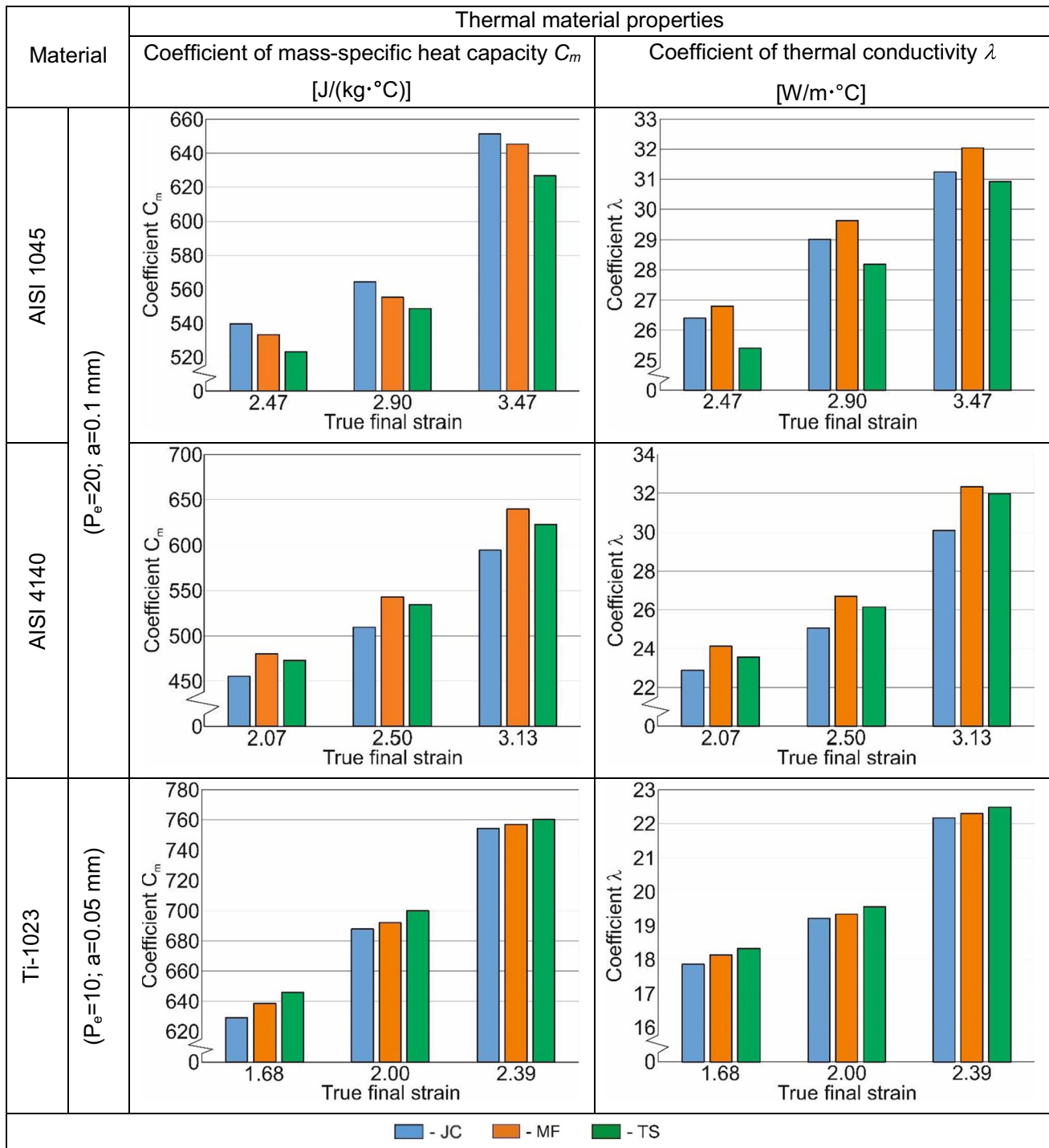
methods can be applied. The decision to use one or another method of determining the tangential stresses is up to the user depending on what data and capabilities he has. In particular, whether data are available on the parameters of the constitutive equation, or whether it is possible to determine cutting forces experimentally, etc. The availability of these data and possibilities determines the type of tangential stress determination method.

The question which calculation variant would be more suitable for establishing the thermal properties should be answered based on the simulation results for the cutting processes. This is dealt with in the next chapter.

7 Simulation of orthogonal cutting processes

In order to verify the elaborated methodology for determining the thermal properties of the machined material and to validate the suggested calculation variants, a FEM modeling and a subsequent simulation of the orthogonal cutting process were carried out. The FEM cutting model was developed in the environment of the commercial software DEFORM 2D/3D^{TM} [83]. The simulation was based on the updated implicit Lagrangian formulation method. It was assumed for all models that the material of the workpiece was isotropic of the plastic type and the material of the tool was rigid. The material model of the three examined materials was based on the constitutive Johnson-Cook equation with the model parameters listed in Table 2. The fracture mechanism of the cutting process was modeled with the damage model by Cockcroft and Latham [84]. The critical elongation for AISI 1045 steel was 210 MPa, 280 MPa for AISI 4140 steel, and 240 MPa for Ti-1023 titanium alloy respectively. These critical stresses were determined with the help of a design of experiments (DOE) analysis [12, 82]. The contact between tool and chip as well as between tool and workpiece was modeled with a hybrid friction model. The friction model was composed of a combination of the Coulomb model and a shear friction model. Regarding the modeling of the cutting processes for AISI 1045 and AISI 4140 steel, the Coulomb coefficient of friction was 0.15 and the plastic proportion of the shear friction model was 0.6. Regarding the modeling of the friction process during the machining of Ti-1023 titanium alloy, the Coulomb coefficient of friction was 0.2 and the shear friction coefficient was 0.8 [12, 82].

Fig. 7 presents the meshed initial geometrical model with boundary conditions. The boundary conditions were determined by fixing the workpiece and the tool as well as by the input of the thermal conditions at the boundaries of the respective objects. The bottom of the workpiece was rigidly fixed in the X-, Y-, and Z-directions. The rigid fixation of the tool at the back of its rake face in Z-direction prevented its meshing in this direction. The thermal initial conditions at room temperature T_r were given at the bottom and the left-hand side of the workpiece as well as at the right-hand side and the top of the tool. The working motion of the tool at a cutting speed V_C for guaranteeing the cutting process was given by the absolute motion in the negative X-direction.

The validity and functionality of the developed numerical cutting model were tested by simulating the cutting process characteristics: chip formation, deformation rate development in the shear zones, as well as temperature flows in the workpiece when machining AISI 1045 and AISI 4140 steels, as well as titanium alloy Ti-1023. The specified cutting characteristics are exemplarily presented in Table 4 for some studied cutting parameters. Analysis of the modeling results of the cutting characteristics showed that the developed model is appropriate for further simulation.

The temperature change during orthogonal cutting at the exterior surface of the chip forming during machining of the studied materials is shown in Fig. 8. The experimental and simulated temperatures depending on the true final strain of the machined material are one above the other here. The depicted results were selected as examples for the cutting parameters which were represented by the Péclet number of $P_e = 20$ for AISI 1045 and AISI 4140 steel as well as $P_e = 10$ for Ti-1023 titanium alloy. The simulations were carried out with the values of the thermal material properties, established according to three variants: (1) due to the yield stress (flow stress) σ_t calculated with the Johnson-Cook constitutive equation (JC), (2) based on the resultant forces F_X and F_Z determined by experiment (MF), and (3) through the direct calculation of tangential stress τ_t (TS). Experimental and simulated temperatures were determined at the same place, shown in the simulation pictures (s. Fig. 8, a, b, and c).

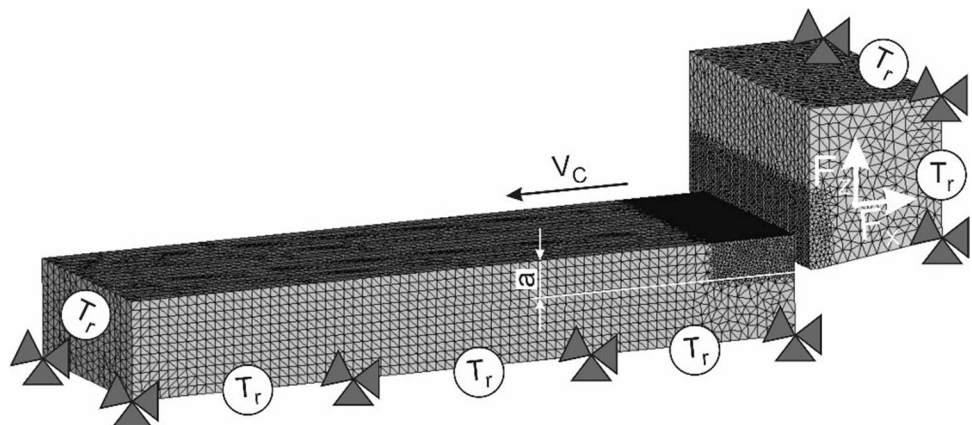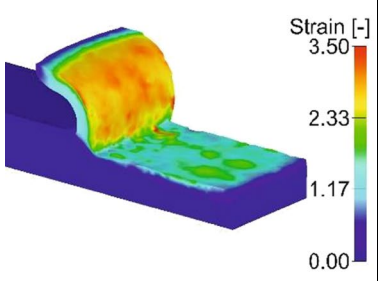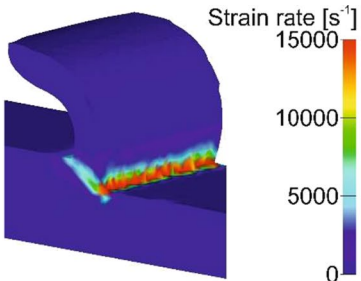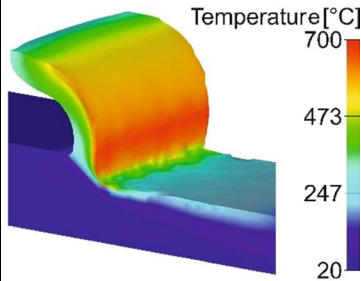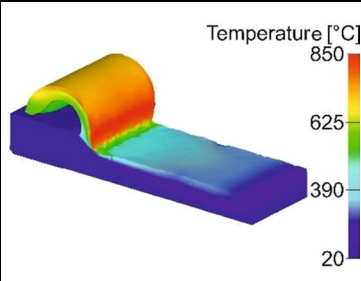**Fig. 7** Initial geometry and boundary conditions of the FEM cutting model
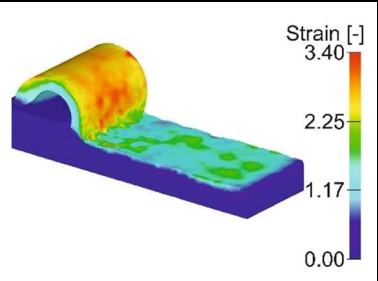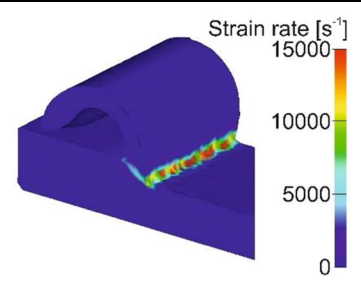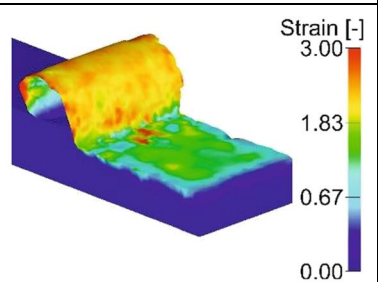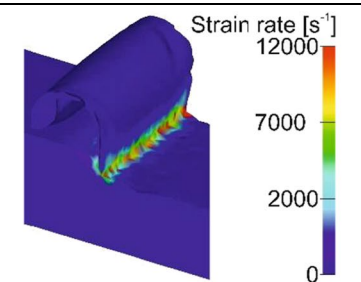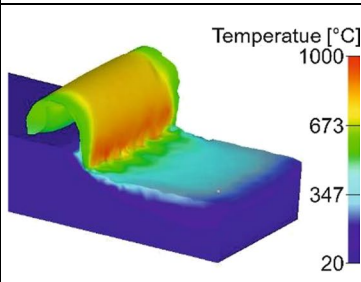
Table 4 Simulation results of the developed numerical cutting model functionality

The temperatures established by the experiment for these cutting parameters ranged from approx. 340 °C up to approx. 470 °C for the three analyzed materials (s. Fig. 8). The temperatures at the exterior surface of the chip in the boundaries of the primary cutting zone were clearly higher in the cutting of the titanium alloy, as already shown in Fig. 6. The temperatures established by simulation showed a good agreement with the corresponding values determined by the experiment. The simulated cutting temperatures deviated from the experimental ones by approx. 7.5 to 14.4%. For all three examined materials, the best agreement was achieved by those temperatures that were simulated based on the thermal properties calculated according to the second variant (MF) (see Fig. 8). That could be explained, as the experimentally determined components of the resultant forces were used in this case to establish the thermal properties of the material.

The greatest deviation occurred in the third variant (TS) for calculating the thermal properties. Nonetheless, this variant also guaranteed a permissible deviation between

the cutting temperatures established by experiment and by simulation.

Hence, the proposed methodology for determining the thermal properties of machined materials offers a reasonably good agreement between the experimental and simulated values of cutting temperatures for the simulation of cutting processes.

8 Conclusion

A methodology for determining the thermal properties of materials under stress-strain conditions corresponding to the loading conditions of the material in the cutting process has been proposed and implemented. This methodology is based on analytical models for determining tangential stresses in the primary cutting zone. Thermal properties of the machined materials, namely the coefficient of specific heat capacity C_m and the coefficient of thermal conductivity λ, were calculated using the developed software algorithm on the basis of tangential stresses in the primary cutting
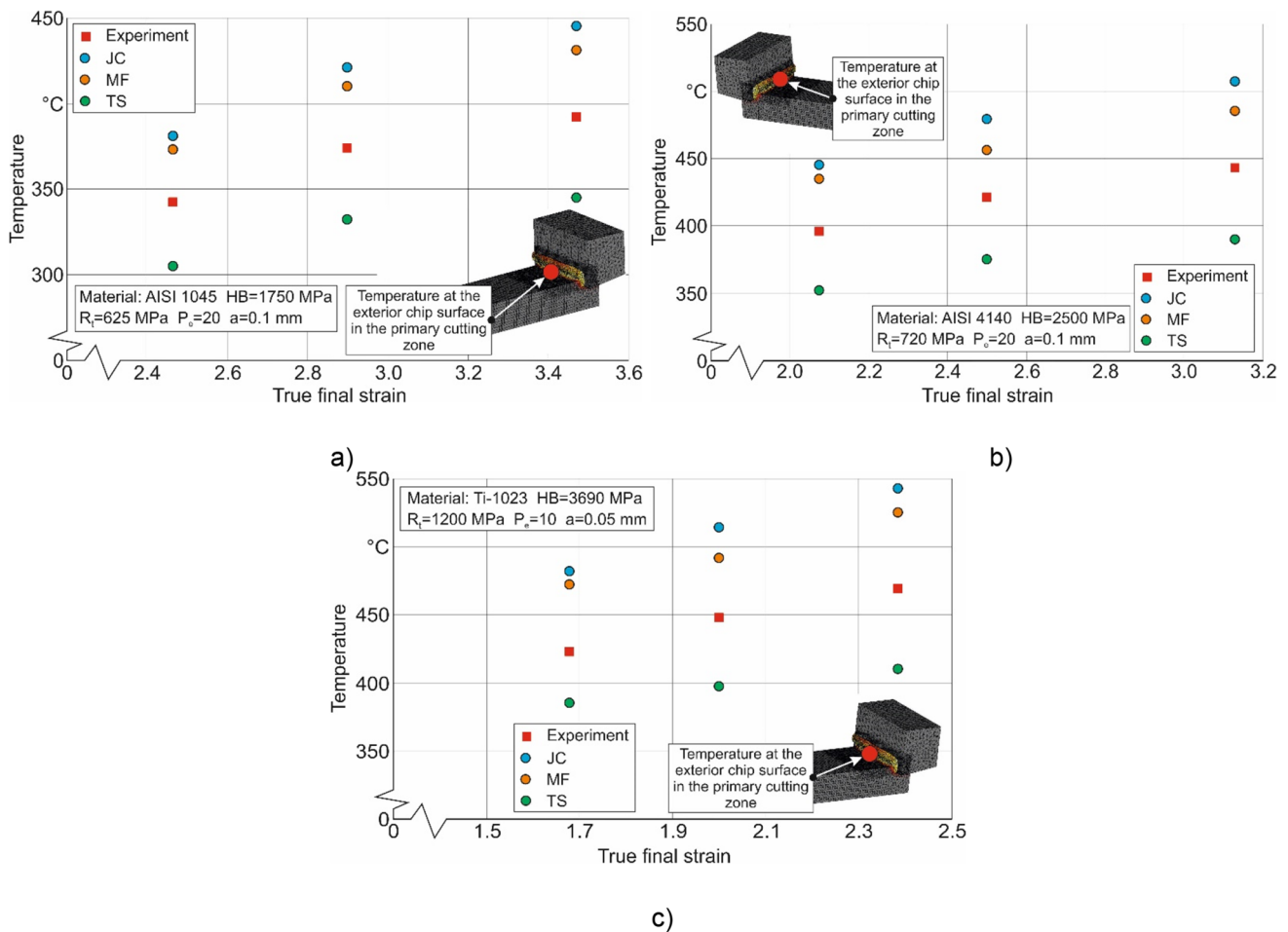
Fig. 8 (**a**, **b**, **c**) Comparison of experimental and simulated temperatures

zone and the cutting temperature in this zone. The algorithm involves using the measured or analytically calculated cutting temperature.

Three methods have been proposed to determine the tangential stresses: by yield strength s_t calculated from the Johnson-Cook equation, on the basis of the resultant forces F_X and F_Z determined experimentally, and by direct calculation of the tangential stress t_t.

The developed methodology was tested on three different materials: AISI 1045 steel, AISI 4140 steel, and titanium alloy Ti-1023 (Ti10V2Fe3Al). The thermal properties of the studied materials for the chosen range of cutting parameters, calculated using the three methods, depend significantly on the Péclet criterion and the true final strain of the material and are proportional to these characteristics. The absence of close correlation in these dependencies allows to conclude that it is necessary to determine the thermal properties of the processed material in each case separately.

The adequacy of the developed methodology for determining the material thermal properties was evaluated by comparing the measured and simulated cutting temperatures. A temperature comparison showed a fairly good match. The experimental temperature values differed from the simulated values by about 7.5 to 14.4%. The smallest deviation was achieved when calculating thermal properties using experimentally determined components of the resulting cutting forces. Thus, it can be stated that the developed methodology can be used to determine the thermal properties of machined materials.

Data availability The data sets supporting the results of this article are included within the article.

Declarations

Ethics approval Not applicable.

Consent to participate Not applicable.

Consent for publication All of the authors have informed us of their consent to the publication of the paper.

Competing interests The authors declare no competing interests.

References

1. Mourtzis D, Doukas M, Bernidaki D (2014) Simulation in manufacturing: review and challenges. Procedia CIRP 25:213–229. https://doi.org/10.1016/j.procir.2014.10.032

2. Afrasiabi M et al (2021) Smoothed particle hydrodynamics simulation of orthogonal cutting with enhanced thermal modeling. Appl Sci 11:1020. https://doi.org/10.3390/app11031020

3. Arrazola PJ, Özel T, Umbrello D, Davies M, Jawahir I (2013) Recent advances in modelling of metal machining processes. CIRP Ann Manuf Technol 62:695–718. https://doi.org/10.1016/j.cirp.2013.05.006

4. Balázs BZ, Geier N, Takács M et al (2021) A review on micromilling: recent advances and future trends. Int J Adv Manuf Technol 112:655–684. https://doi.org/10.1007/s00170-020-06445-w

5. Li J, et al (2021) An experimental and finite element investigation of chip separation criteria in metal cutting process. International Journal of Advanced Manufacturing Technology. 10.1007/s00170-021-07461-0.

6. Grzesik W (2020) Modelling of heat generation and transfer in metal cutting: a short review. J Mach Eng 20(1):24–33. https://doi.org/10.36897/jme/117814

7. Courbon C et al (2021) A 3D modeling strategy to predict efficiently cutting tool wear in longitudinal turning of AISI 1045 steel. CIRP Ann 70(1):57–60. https://doi.org/10.1016/j.cirp.2021.04.071

8. Liu Y et al (2021) Investigation on residual stress evolution in nickel-based alloy affected by multiple cutting operations. J Manuf Process 68, Part A:818–833. https://doi.org/10.1016/j.jmapro.2021.06.015

9. Eivani AR et al (2021) A novel approach to determine residual stress field during FSW of AZ91 Mg alloy using combined smoothed particle hydrodynamics/neuro-fuzzy computations and ultrasonic testing. J Magnes Alloys 9(4):1304–1328. https://doi.org/10.1016/j.jma.2020.11.018

10. Heisel U et al (2009) Thermomechanical material models in the modeling of cutting processes. ZWF Z fuer Wirtsch Fabr 104(6):482–491. (In German). https://doi.org/10.3139/104.110104

11. Özel T, Zeren EA (2006) A Methodology to determine work material flow stress and tool-chip interfacial friction properties by using analysis of machining. ASME J Manuf Sci Eng 128(1):119–129. https://doi.org/10.1115/1.2118767

12. Storchak M, Rupp P, Möhring H-C, Stehle T (2019) Determination of Johnson–Cook constitutive parameters for cutting simulations. Metals 9(4):473. https://doi.org/10.3390/met9040473

13. Melkote SN (2017) et. al.: Advances in material and friction data for modeling of metal machining. CIRP Ann 66(2):731–754. https://doi.org/10.1016/j.cirp.2017.05.002

14. Heisel U et al (2009) Thermomechanical exchange effects in machining. ZWF Z für Wirtsch Fabr 104(4):263–272. https://doi.org/10.3139/104.110016

15. Saelzer J et al (2021) Modelling of the friction in the chip formation zone depending on the rake face topography. Wear 477:203802. https://doi.org/10.1016/j.wear.2021.203802

16. Heisel U et al (2009) Breakage models for the modeling of cutting processes. ZWF 104(5):330–339 (In German). https://doi.org/10.3139/104.110057

17. Buchkremer S, Schoop J (2016) A mechanics-based predictive model for chip breaking in metal machining and its validation. CIRP Ann 65(1):69–72. https://doi.org/10.1016/j.cirp.2016.04.089

18. Sela A et al (2021) Inverse identification of the ductile failure law for Ti6Al4V based on orthogonal cutting experimental outcomes. Metals 11:1154. https://doi.org/10.3390/met11081154

19. Zhang C, Choi H (2021) Study of segmented chip formation in cutting of high-strength lightweight alloys. Int J Adv Manuf Technol 112:2683–2703. https://doi.org/10.1007/s00170-020-06057-4

20. Zhang J et al (2021) Fragmented chip formation mechanism in high-speed cutting from the perspective of stress wave effect. CIRP Ann 70(1):53–56. https://doi.org/10.1016/j.cirp.2021.03.016

21. Barzegar Z, Ozlu E (2021) Analytical prediction of cutting tool temperature distribution in orthogonal cutting including third deformation zone. J Manuf Process 67:325–344. https://doi.org/10.1016/j.jmapro.2021.05.003

22. Storchak M, Kushner V, Möhring H-C, Stehle T (2021) Refinement of temperature determination in cutting zones. J Mech Sci Technol 35(8). https://doi.org/10.1007/s12206-021-0736-4

23. Osorio-Pinzon JC, Abolghasem S, Casas-Rodriguez JP (2019) Predicting the Johnson-Cook constitutive model constants using temperature rise distribution in plane strain machining. Int J Adv Manuf Technol 105(1-4):279–294. https://doi.org/10.1007/s00170-019-04225-9

24. Hu C et al (2020) Cutting temperature prediction in negative-rake-angle machining with chamfered insert based on a modified slip filed model. Int J Mech Sci 167:105273. https://doi.org/10.1016/j.ijmecsci.2019.105273

25. Kumar A, Bhardwaj R, Joshi SS (2020) Thermal modeling of drilling process in titanium alloy (Ti-6Al-4V). Mach Sci Technol 24(3):341–365. https://doi.org/10.1080/10910344.2019.1698607

26. Tu L et al (2019) Temperature distribution of cubic boron nitride–coated cutting tools by finite element analysis. Int J Adv Manuf Technol 105(7-8):3197–3207. https://doi.org/10.1007/s00170-019-04498-0

27. Davies MA, Ueda T, M'Saoubi R, Mullany B, Cooke AL (2007) On the measurement of temperature in material removal processes. CIRP Ann 56(2):581–604. https://doi.org/10.1016/j.cirp.2007.10.009

28. Özel T, Altan T (2000) Determination of workpiece stress and friction at the chip-tool contact for high speed cutting. J Mach Tools Manuf 40:133–152. https://doi.org/10.1016/S0890-6955(99)00051-6

29. Abukhshim MA, Mativenga PT, Sheikh MA (2006) Heat generation and temperature prediction in metal cutting: a review and

30. Biermann D, Hollmann F (2018) Thermal effects in complex machining processes. Final Report of the DFG Priority Programme 1480. Springer. https://doi.org/10.1007/978-3-319-57120-1

31. Ebrahimi SM, Araee A, Hadad M (2019) Investigation of the effects of constitutive law on numerical analysis of turning processes to predict the chip morphology, tool temperature, and cutting force. Int J Adv Manuf Technol 105(10):4245–4264. https://doi.org/10.1007/s00170-019-04502-7

32. Ribeiro-Carvalho S, Horovistiz A, Davim JP (2021) Material model assessment in Ti6Al4V machining simulations with FEM. Proceedings of the Institution of Mechanical Engineers, Part C: Journal of Mechanical Engineering Science, p. 095440622199488. https://doi.org/10.1177/0954406221994883

33. Hu C, Zhuang K, Weng J, Pu D (2019) Three-dimensional analytical modeling of cutting temperature for round insert considering semi-infinite boundary and non-uniform heat partition. Int J Mech Sci 155:536–553. https://doi.org/10.1016/j.ijmecsci.2019.03.019

34. Chen Y, Li H, Wang J (2015) Further development of Oxley's predictive force model for orthogonal cutting. Mach Sci Technol 19(1):86–111. https://doi.org/10.1080/10910344.2014.991026

35. Crichigno Filho JM (2017) Applying extended Oxley's machining theory and particle swarm optimization to model machining forces. Int J Adv Manuf Technol 89(1-4):1127–1136. https://doi.org/10.1007/s00170-016-9155-6

36. Huang Y, Liang SY (2003) Cutting forces modeling considering the effect of tool thermal property—application to CBN hard turning. Int J Mach Tool Manu 43(3):307–315. https://doi.org/10.1016/S0890-6955(02)00185-2

37. Kronenberg M (1966) Machining science and application: theory and practice for operation and development of machining processes. Oxford: Pergamon Pr, 410 p

38. Mills KC (2002) Recommended values of thermophysical properties for selected commercial alloys. Woodhead Published Lim., Cambridge England, 244 p

39. Craviero H (2016) D. et. al.: Review of the high temperature mechanical and thermal properties of the steel used in cold formed steel structures — the case of the S280 Gd+Z steel. Thin-Walled Struct 98:154–168. https://doi.org/10.1016/j.tws.2015.06.002

40. Franssen JM, Real PV (2015) Fire design of steel structures. 2nd edn, Wiley Ernst & Sohn, Berlin, 2015, 450 p.

41. Fang H, Wong WB, Bai Y (2015) Use of kinetic model for thermal properties of steel at high temperatures. Aust J Civ Eng 13(1):40–47. https://doi.org/10.1080/14488353.2015.1092637

42. Wielgosz E, Kargul T, Falkus J (2014) Comparison of experimental and numerically calculated thermal properties of steels. Conference "Metal 2014", Brno, Chech Republic, May 2st – 23rd

43. Choi I-R, Chung K-S, Kim D-H (2014) Thermal and mechanical properties of high-strength structural steel HSA800 at elevated temperatures. Mater Des 63:544–551. https://doi.org/10.1016/j.matdes.2014.06.035

44. Chen Z, Lu J, Liu H, Liao X (2016) Experimental study on the post-fire mechanical properties of high-strength steel tie rods. J Constr Steel Res 121:311–329. https://doi.org/10.1016/j.jcsr.2016.03.004

45. Gardner, L. et. al. Elevated temperature material properties of stainless steel reinforced bar. Constr Build Mater, 2016, Vol. 114, pp. 977 – 997. https://doi.org/10.1016/j.conbuildmat.2016.04.009.

46. Fan, S. et. al. Experimental investigation of austenitic stainless steel material at elevated temperatures. Constr Build Mater, 2017, Vol. 155, pp. 267 – 285. https://doi.org/10.1016/j.conbuildmat.2017.08.047.

47. Díaz-Álvarez J, Tapetado A, Vázquez C, Miguélez H (2017) Temperature measurement and numerical prediction in machining Inconel 718. Sensors 17(7):1531. https://doi.org/10.3390/s17071531

48. Michna J (2014) Numerical and experimental investigation of cutting-induced microstructure transformation and modeling of the thermo-mechanical load collective when drilling 42CrMo4. Dissertation, Institute for Technology, Karlsruhe, 196 p

49. Attanasio A, Umbrello D (2009) Abrasive and diffusive tool wear FEM simulation. Int J Mater Form 2(1):543–546. https://doi.org/10.1007/s12289-009-0475-z

50. Oxley PLB (1989) Mechanics of Machining. An analytical approach to assessing machinability. Ellis Horwood: Chichester, UK; 242 p. https://doi.org/10.1115/1.2888318

51. Zorev NN (1966) Metal cutting mechanics. Pergamon Press GmbH: Frankfurt am Main, Germany; 526 p.

52. Kushner V, Storchak M (2017) Modelling the material resistance to cutting. Int J Mech Sci 126:44–54. https://doi.org/10.1016/j.ijmecsci.2017.03.024

53. Möhring H-C, Kushner V, Storchak M, Stehle T (2018) Temperature calculation in cutting zones. CIRP Ann 67(1):61–64. https://doi.org/10.1016/j.cirp.2018.03.009

54. Grzesik W (2006) Determination of temperature distribution in the cutting zone using hybrid analytical-FEM technique. Int. J Mach Tools Manuf 46(6):651–658. https://doi.org/10.1016/j.ijmachtools.2005.07.009

55. Heisel U, Storchak M, Eberhard P, Gaugele T (2011) Experimental studies for verification of thermal effects in cutting. Prod Eng 5(5):507–515. https://doi.org/10.1007/s11740-011-0312-3

56. Kushner V, Storchak M (2014) Determining mechanical characteristics of material resistance to deformation in machining. Prod Eng 8(5):679–688. https://doi.org/10.1007/s11740-014-0573-8

57. Chao BT, Trigger KJ (1958) Temperature distribution at tool-chip and tool-work interface in metal cutting. Trans ASME 80:311–320

58. Heisel U, Storchak M, Krivoruchko D (2013) Thermal effects in orthogonal cutting. Prod Eng 7(2):203–211. https://doi.org/10.1007/s11740-013-0451-9

59. Johnson GR, Cook WH A constitutive model and data for metals subjected to large strains, high strain and high temperatures. In Proceedings of the 7th International Symposium on Ballistics, The Hague, The Netherlands, 19–21 April 1983, pp. 541–547

60. Adibi-Sedeh AH, Madhavan V, Bahr B (2003) Extension of Oxley's analysis of machining to use different material models. J Manuf Sci Eng 125(4):656–666. https://doi.org/10.1115/1.1617287

61. Lalwani DI, Mehta NK, Jain PK (2009) Extension of Oxley's predictive machining theory for Johnson-and Cook flow stress model. J Mater Process Technol 209(12-13):5305–5312. https://doi.org/10.1016/j.jmatprotec.2009.03.020

62. Xiong L, Wang J, Gan Y, Li B, Fang N (2015) Improvement of algorithm and prediction precision of an extended Oxley's theoretical model. Int J Adv Manuf Technol 77:1–13. https://doi.org/10.1007/s00170-014-6361-y

63. Laakso SVA, Niemi E (2016) Modified Johnson-Cook flow stress model with thermal softening damping for finite element modeling of cutting. J Eng Manuf 230(2):241–253. https://doi.org/10.1177/0954405415619873

64. Calamaz M, Coupard D, Girot F (2008) A new material model for 2D numerical simulation of serrated formation when machining titanium alloy Ti-6Al-4V. Int J Mach Tools Manuf 48(3-4):275–288. https://doi.org/10.1016/j.ijmachtools.2007.10.014

65. Denguir LA, Outeiro JC, Fromentin G, Vignal V, Besnard R (2016) Orthogonal cutting simulation of OFHC copper using a new constitutive model considering the state of stress and the

microstructure effects. Procedia CIRP 46:238–241. https://doi.org/10.1016/j.procir.2016.03.208

66. Heisel U, Kushner V, Storchak M (2012) Effect of machining conditions on specific tangential forces. Prod Eng 6(6):621–629. https://doi.org/10.1007/s11740-012-0417-3

67. Barrow G (1973) A review of experimental and theoretical techniques for assessing cutting temperatures. CIRP Ann 22(2):203–211

68. Burns GW, Scroger MG (1989) The calibration of thermocouples and thermocouple materials. National Institute of Standards and Technology, 201 p.

69. Kus A, Isik Y, Cakir MC, Coşkun S, Özdemir K (2015) Thermocouple and infrared sensor-based measurement of temperature distribution in metal cutting. Sensors 15(1):1274–1291. https://doi.org/10.3390/s150101274

70. Cui Y, Yang D, Jia Y, Zeng Q, Sun B (2011) Dynamic calibration of the cutting temperature sensor of NiCr/NiSi thin-film thermocouple. Chin J Mech Eng 24(1):73–77. https://doi.org/10.3901/CJME.2011.01.073

71. Dhar NR, Islam S, Kamruzzaman M, Ahmed T (2005) The calibration of tool-work thermocouple in turning steels. Conference Modeling, Simulation and Control of Engineering Systems, pp. 459–466.

72. Kaminise AK, Guimarães J, da Silva MB (2014) Development of a tool–work thermocouple calibration system with physical compensation to study the influence of tool-holder material on cutting temperature in machining. Int J Adv Manuf Technol 73(5–8):735–747. https://doi.org/10.1007/s00170-014-5898-0

73. Nedić BP, Erić MD (2014) Cutting temperature measurement and material machinability. Therm Sci 18(1):259–268. https://doi.org/10.2298/TSCI120719003N

74. Noriega M, Ramírez R, López R, Vaca M, Morales J, Terres H, Lizardi A, Chávez S (2015, 012029) Thermocouples calibration and analysis of the influence of the length of the sensor coating. J Phys Conf Ser 582:1–6. https://doi.org/10.1088/1742-6596/582/1/012029

75. Sutter G, Ranc N (2007) Temperature fields in a chip during high-speed orthogonal cutting — an experimental investigation. Int J Mach Tools Manuf 47(10):1507–1517. https://doi.org/10.1016/j.ijmachtools.2006.11.012

76. Muller B (2001) Temperature measurements with a fibre-optic two-colour pyrometer. In: H. Schulz (Ed.), Scientific Fundamentals of High Speed Cutting, Carl Hanser Verlag, München, pp.: 181–186. https://publications.rwth-aachen.de/record/87014.

77. Tapetado A et al (2016) Two-color pyrometer for process temperature measurement during machining. J Lightwave Technol 34(4):1380–1386. https://doi.org/10.1109/JLT.2015.2513158

78. Sutter G et al (2003) An experimental technique for the measurement of temperature fields for the orthogonal cutting in high speed. Int J Mach Tools Manuf 43(7):671–678. https://doi.org/10.1016/S0890-6955(03)00037-3

79. Lis K, Kosmol J (2008) Temperature monitoring of the drilling process using thermovision method. 12th International Research/Expert Conference "Trends in the Development of Machinery and Associated Technology" TMT 2008, Istanbul, Turkey, 26-30 August, 2008, pp. 113 – 116.

80. Ranc N, Pina V, Sutter G, Philippon S (2004) Temperature measurement by visible pyrometry: orthogonal cutting application. J Heat Transf Am Soc Mech Eng 126(6):931–936. https://doi.org/10.1115/1.1833361

81. Soler D, Aristimuño PX, Saez-de-Buruaga M, Arrazola PJ (2019) Determination of emissivity and temperature of tool rake face when cutting AISI 4140. Procedia Manuf 41:304–311. https://doi.org/10.1016/j.promfg.2019.09.013

82. Storchak M, Jiang L, Xu Y, Li X (2016) FEM modelling for the cutting process of the titanium alloy Ti10V2Fe3Al. Prod Eng 10:509–517. https://doi.org/10.1007/s11740-016-0689-0

83. Deform-User Manual SFTC-Deform V12.0, Columbus (OH), USA, 2019.

84. Cockcroft MG, Latham DJ (1968) Ductility and workability of metals. J Inst Met 96:33–39